J of Nuclear Medicine Technology, first published online February 7, 2023 as doi:10.2967/jnmt.122.264909

# Evaluation of data-driven respiratory gating in continuous bed motion in lung lesions

Takeshi Nii[1], Shota Hosokawa[2], Tomoya Kotani[3], Hiroshi Domoto[1], Yasunori Nakamura[1], Yasutomo Tanada[1], Ryotaro Kondo[1], Yasuyuki Takahashi[2]

[1] Department of Medical Technology, Division of Radiological Technology, University Hospital, Kyoto Prefectural University of Medicine, 465 Kajii-cho, Kamigyo-ku, Kyoto, 602-8566, Japan

[2] Department of Radiation Science, Graduate School of Health Sciences, Hirosaki University, 66-1 Hon-cho, Hirosaki 036-8564, Japan

[3] Department of Radiology, Graduate School of Medical Science, Kyoto Prefectural University of Medicine, 465 Kajii-cho, Kamigyo-ku, Kyoto, 602-8566, Japan

Correspondence: Takeshi Nii,

Department of Medical Technology, Division of Radiological Technology, University Hospital, Kyoto Prefectural University of Medicine, 465 Kajii-cho, Kamigyo-ku, Kyoto, 602-8566, Japan

Tel +81-75-251-5628, Fax +81-75-251-5628,

E-mail: nii21@koto.kpu-m.ac.jp

ORCID 0000–0003–0409–8378

Financial support: None

Short title: data-driven respiratory gating PET/CT

## Abstract

**Objectives** Respiratory gating is used in positron emission tomography (PET) to prevent image quality degradation due to respiratory effects. In this study, we evaluated a data-driven respiratory gating for continuous bed motion OncoFreeze AI, which was implemented to improve image quality and accuracy of semiquantitative uptake values affected by respiratory motion.

**Methods** $^{18}$F-fluoro-deoxyglucose PET/ computed tomography was performed on 32 patients with lung lesions. Two types of respiratory gating images (OncoFreeze AI with data-driven respiratory gating, device-based amplitude-based OncoFreeze with elastic motion compensation) and ungated images (Static) were reconstructed. For each image, we calculated standardized uptake value (SUV) and metabolic tumor volume (MTV). The improvement rate (IR) from respiratory gating and the contrast-to-noise ratio (CNR), which indicates the improvement in image noise, were also calculated for these indices. IR was also calculated for the upper and lower lobes of the lung. As OncoFreeze AI assumes the presence of respiratory motion, we examined quantitativity in regions where respiratory motion was not present using a $^{68}$Ge cylinder phantom with known quantitativity.

**Results** OncoFreeze and OncoFreeze AI showed similar values, with a significant increase in SUV and decrease in MTV compared to Static. OncoFreeze and OncoFreeze AI also showed similar values for IR and CNR. OncoFreeze AI increased SUVmax by an average of 18% and decreased MTV by an average of 25% compared to Static. From the IR results, both OncoFreeze and OncoFreeze AI showed a greater

improvement rate from Static in the lower lobe than in the upper lobe.

OncoFreeze and OncoFreeze AI increased CNR by 17.9% and 18.0%, respectively, compared to Static. The quantitativity of the $^{68}$Ge phantom, assuming a region of no respiratory motion, was almost equal for the Static and OncoFreeze AI.

**Conclusions** OncoFreeze AI improved the influence of respiratory motion in the assessment of lung lesion accumulation to a comparable level to the previously launched OncoFreeze. OncoFreeze AI provides more accurate imaging with significantly larger SUV values and smaller MTV than Static.

**Key words:** Data driven gating, Lung lesions, FDG, PET/CT

## Introduction

$^{18}$F-fluorodeoxyglucose (FDG) positron emission tomography/computed tomography (PET/CT) is useful in the stage, restage and assess treatment response of lung cancer (*1, 2*). Respiration affects the evaluation of lung lesions, which extends to blurred images, standardized uptake value (SUV), and metabolic tumor volume (MTV) (*3–6*). It has been reported that the respiratory motion of the lungs is greater in the lower lobe than in the upper lobe by a maximum of 6 to 12 cm (*7, 8*). As an imaging biomarker, SUV is highly reproducible and ideal for monitoring tumor response to treatment in individual patients (*9*). But the reliability of FDG-PET as a treatment response assessment is compromised if these indices, which monitor tumor responsiveness in areas affected by respiratory motion and areas not affected by respiratory motion, cannot be evaluated equivalently.

To solve these problems, a respiratory gating scan method has been developed to detect breathing motion using a device (*10, 11*). This captures respiration as a waveform and detects the expiratory phase to get a low motion image. However, as only the expiration phase is used from the collected data, the scan time is extended. A mechanism was proposed that combined amplitude-based PET gating with elastic motion correction for comprehensive respiratory management (*12*). Based on the spectral analysis method (SAM) developed for single-bed position PET imaging, respiratory gate imaging can be performed with device-less waveforms that derive waveforms directly from PET list mode raw data (*13, 14*). Several different approaches at deviceless waveform generation for PET have been robustly demonstrated on single-bed-

position PET (*14–16*). The deviceless waveform in the multi-bed position was first realized by step-and-shoot collection (*17*).

OncoFreeze is a respiratory gating software that combines continuous bed motion (CBM) and device-based amplitude-based PET gating with elastic motion compensation (*12*). OncoFreeze AI, a data-driven device-less respiratory gating system (DDG) by CBM systems, was later created (*18, 19*). The purpose of this study was to verify the usefulness of OncoFreeze AI and OncoFreeze in lung lesions.

## Materials and methods

The Institutional Review Board and Ethics Committee of Kyoto Prefectural University of Medicine, Japan (ERB-C-2578) approved this retrospective study and the requirement to obtain informed consent was waived. Thirty-eight lesions in 32 lung cancer patients who underwent $^{18}$F-FDG respiratory gated PET/CT between January 2022 and May 2022 were included. Thirty-eight lesions were included, consisting of 18 in the upper lobe, five in the middle lobe, and 15 in the lower lobe. The mean age of the patients was 73.7 years (50-93), 20 males and 12 women, body mass index was 22.28 ± 3.62, and the dose of FDG was 202.28 ± 25.79 MBq (3.61 ± 0.65 MBq/Kg). PET/CT examination was performed as follows. Prior to FDG injection, the patients fasted for > 4 h, and their blood glucose levels were below 200 mg/dl. Each patient received FDG using an automatic injection system (Auto Dispensing Injector UG-05, Universal

Giken Co. Ltd., Odawara, Japan). PET/CT imaging was performed at 60 min after FDG injection using a PET/CT system (Biograph Horizon 4R, Siemens Medical Solutions, Knoxville, TN, USA). FDG-PET imaging was performed using CBM at varying speeds (1.5 mm/s from the head to the pelvis, and 3.5 mm/s for the lower limbs). During examination, the belt gating (BG) system AZ-733VI (Anzai Medical, Co. Ltd, Tokyo, Japan) recorded respiratory signals that were used for gating. PET images were reconstructed using a three-dimensional ordered subset expectation maximization coupled with point–spread–function and time–of–flight algorithms. The following clinical parameters were set: four iterations, 10 subsets, 5-mm (FWHM) post-reconstruction Gaussian filter, and 180 × 180-pixel matrix (pixel size = 4 mm). Low-dose CT scan was acquired for PET attenuation correction, anatomical information, and image fusion with the following scanning parameters: tube voltage, 130 kV; quality reference mAs, 90; rotation time, 0.6 s; pitch, 1.5; slice thickness, 2.0 mm; transaxial field of view, 700 mm; and matrix size, 512 × 512. In the chest, respiratory gating reconstruction and static reconstruction (Static) were performed. Respiratory gating reconstruction was performed with device-less OncoFreeze AI and device-based OncoFreeze. OncoFreeze is a new respiratory gating function based on HD-Chest technology that does not require an increase in imaging time. OncoFreeze uses mass preserving optical flow to generalize respiratory motion and reconstructs the image using all count data from the HD-Chest image as a reference. OncoFreeze AI is a device-less respiratory gating method that extracts respiratory waveforms for each patient from continuous PET data using Flow Motion, and reconstructs respiratory gating images based on those

respiratory waveforms. OncoFreeze AI uses DDG to estimate the respiratory waveform in a device-less manner using the following procedure based on the features of DDG and Flow Motion. Estimate the respiratory waveform using the change in the Anterior-Posterior direction from the PET data collected by Flow Motion (Resp Curve A). The PET data is divided into 500 msec volumes. Fourier transform the PET data with respect to time. Fourier transform Resp Curve A to determine the conditions (frequency and range) to be used in the SAM. Calculate each PET data in the SAM and create a mask for each voxel to compensate for the effect of respiration. Apply the mask to the temporally segmented volume data to generate a respiratory waveform (Resp Curve B). Normalize Resp Curve B. Compare Resp Curve A and B to create a waveform that matches the actual respiratory motion. This produces a device-less respiratory waveform and allows for respiratory-gated image reconstruction (*18, 19*).

OncoFreeze AI and OncoFreeze are software that is equipped on the Biograph Horizon 4R (*19*).

For each reconstruction algorithm, SUVmax, SUVpeak, and MTV were measured; the threshold for MTV was set at 40% SUVmax. SUVs were calculated using body weight. MTV unit is $cm^3$.

The improvement rate (IR) over Static with respiratory gating was calculated for SUVmax, SUVpeak, and MTV.

The IR (IRSmax) of SUVmax for OncoFreeze AI was calculated using the following formula.

$$\text{IRSmax (\%)} = \frac{(\text{OncoFreeze AI} - \text{Static})}{\text{Static}} \times 100 . \qquad \text{Eq. 1}$$

The same formula was also used to calculate IR (IRSpeak) of SUVpeak, IR (IRMTV) of MTV. And

OncoFreeze was calculated in the same way.

Contrast-to-noise ratio (CNR) was calculated using Equation 2.

SUV SD (a surrogate for image noise) was measured using a 3-cm-diameter spheric region of interest in the lung that we assessed to be free of disease. CNR for each sphere was also calculated according to Equation 2 using the lesion SUVmax (SUVmax, le), background sphere SUVmax (SUVmax, bs), and background sphere SUV SD (sd).

$$\text{CNR} = \frac{(\text{SUVmax,le} - \text{SUVmax,bs})}{\text{sd}} . \qquad \text{Eq. 2}$$

The respiratory rate of the DDG-generated waveform was compared to the respiratory rate accepted by the waveform device. The accepted respiratory rate is recorded on the PET device.

$^{68}$Ge cylinder phantom CS-27 with a volume of 8407 mL, radius of 10 cm, and radioactivity of 73.01 MBq, 8.68kBq/mL (Siemens Medical Solutions, Knoxville, TN, USA) was used to examine the quantitative accuracy in those areas where OncoFreeze AI was applied that were largely unaffected by respiratory motion. PET data were acquired at bed speeds of 0.6–3.0 mm/s (0.3 mm/s increments). A large volume of interest (VOI) was constructed in the center to avoid partial volume and edge effects, and the mean, maximum, and standard deviation (SD) of SUV and radioactivity (Bq/mL) were calculated. These indices were determined by using syngo.via (Siemens Medical Solutions, Knoxville, TN, USA).

All statistical analyses were performed with EZR (Saitama Medical Center, Jichi Medical University,

Saitama, Japan), which is a graphical user interface for R (The R Foundation for statistical Computing, Vienna, Austria) designed to add statistical functions frequently used in biostatistics (*20*).

The significance of SUVmax, SUVpeak, MTV, and CNR were determined by Wilcoxon signed-rank test and Bonferroni adjustment, and IRSmax, IRSpeak, and IRMTV were determined by Mann-Whitney U test, and the waveform respiration rate were determined by paired t-test.

## Results

SUVmax, SUVpeak, and MTV calculated by OncoFreeze AI were almost the same as OncoFreeze. Compared to Static, SUVmax and SUVpeak showed an increase and MTV showed a decrease (Figs. 1–3). SUVmax for Static, OncoFreeze, and OncoFreeze AI was 7.08 ± 1.11, 8.40 ± 1.28, and 8.39 ± 1.31, respectively; SUVpeak was 5.18 ± 0.86, 5.67 ± 0.93, and 5.70 ± 0.95, respectively; MTV was 10.73 ± 1.96, 8.31 ± 1.56, and 8.05 ± 1.51, respectively (mean ± standard error). SUVmax, SUVpeak, and MTV of OncoFreeze AI and OncoFreeze showed good correlation (Fig. 4).

IRSmax, which represents the improvement in SUVmax, was 18.3 ± 2.6% (mean ± standard error) for OncoFreeze and 17.9 ± 2.2% for OncoFreeze AI. IRSpeak was 9.7 ± 1.3% for OncoFreeze and 9.6 ± 1.3% for OncoFreeze AI. IRMTV was -24.2 ± 3.2% for OncoFreeze and -25.5 ± 2.9% for OncoFreeze AI. IRSmax in the upper and lower lobes was 12.0 ± 2.2% and 26.7 ± 5.2% for OncoFreeze and 13.9 ± 2.2%

and 23.8 ± 4.3% for OncoFreeze AI. IRSpeak in the upper and lower lobes was 7.5 ± 1.0% and 13.3 ± 2.9% for OncoFreeze and 7.4 ± 1.1% and 12.9 ± 2.7% for OncoFreeze AI, respectively. IRMTV in the upper and lower lobes was -17.2 ± 3.9% and -33.7 ± 5.7% for OncoFreeze and -22.1 ± 3.8% and -32.1 ± 5.2% for OncoFreeze AI, respectively (Figs. 5, 6). Only the IRSmax of OncoFreeze showed a significant difference between the upper and lower lobes (P = 0.0273); otherwise, there were no significant differences between the upper and lower lobes for both OncoFreeze and OncoFreeze AI.

CNR was significantly higher for OncoFreeze and OncoFreeze AI compared to Static (Fig. 7). The percentage increases for CNR in comparison to Static for OncoFreeze, OncoFreeze AI were 17.9% and 18.0%, respectively. In OncoFreeze AI and OncoFreeze, the number of breaths in the generated waveform is expressed in units of counts. This represents the number of breaths. The respiratory rate of the DDG-generated waveform (OncoFreeze AI) was 223.7 ± 31.2 counts (mean ± standard error) and the respiratory rate accepted by the waveform device (OncoFreeze) was 218.0 ± 52.5 counts, and no significant differences were found (p=0.602). The correlation of the accepted respiratory rate was y=1.31x-76.57 with correlation coefficient $R^2 = 0.61$ (x: OncoFreeze AI, y: OncoFreeze).

The effect of OncoFreeze AI on quantitative accuracy was examined using a $^{68}$Ge cylinder phantom, assuming a region of unchanged counts, and the mean SUV of VOI was 1.04 for both Static and OncoFreeze AI, regardless of bed speed. On the other hand, SUVmax for both Static and OncoFreeze AI increased slightly with increasing bed speed. SUVmax was slightly higher for OncoFreeze AI than for

Static. The SUVmax of OncoFreeze AI, when the SUVmax of Static was set to 1, averaged 1.05 ± 0.02, showing little deviation from the increase in SUVmax of Static with increasing bed speed. The radioactivity at the acquisition date, calculated from the radioactivity at the assay date, was 8.68 (kBq/mL), and the mean radioactivity of Static and OncoFreeze AI was 9.06 ± 0.01 (kBq/mL) and 9.02 ± 0.02 (kBq/mL) (Table 1).

## Discussion

We compared OncoFreeze AI, a device-less respiratory gating system of continuous bed motion imaging with OncoFreeze, which uses devices, on the Biograph Horizon, a commercially available general-purpose PET/CT machine. OncoFreeze AI is a reconstruction method that combines CBM and DDG. Reports so far have not investigated popular PET/CT systems and instead have focused on the high-end Biograph mCT and semiconductor PET, Biograph Vision (*18, 21*). In this study, we found that the OncoFreeze AI on the Biograph Horizon had the same SUVmax, SUVpeak, and MTV in lung lesions as OncoFreeze (Fig. 4).

Respiratory motion is greater in the lower lobe than in the upper lobe (*4*). Based on IRSmax, IRSpeak, and IRMTV, there was a trend toward greater correction effect of respiratory motion in the lower lobe than in the upper lobe. However, there was no significant difference in the correction effect between the upper and lower lobes, except for IRSmax in OncoFreeze ($P = 0.0273$) (Figs. 5, 6). Robin et al. reported a greater

increase in SUV and decrease in MTV in the lower lobe than in the upper lobe due to the correction effect of respiratory motion in amplitude-based respiratory gate HD・Chest® imaging (*6*). In the present study, the same trend was observed for both OncoFreeze, which combines CBM with elastic motion compensation and device-based amplitude-based PET gating, and OncoFreeze AI, which combines a CBM system with a DDG system.

Meier et al. used CNR as a metric to capture both SUVmax and noise. Their study reported a decrease in CNR with correction methodologies that use decreasing amounts of PET data; however, in lung lesions, the elastic motion deblurring algorithm improved the CNR of the lesion by 17.8% with the least increase in image noise (*22*). In the present study, OncoFreeze and OncoFreeze AI, which did not involve a decrease in PET data, showed a significant increase in CNR (17.9% and 18.0%, respectively). The fact that the respiratory rate generated by OncoFreeze AI, which generates respiratory waveforms without a device, was not significantly different from the respiratory rate measured by the device also indicates the usefulness of OncoFreeze AI.

OncoFreeze AI, a development of OncoFreeze, is a device-less method; thus, the waveforms generated are completely dependent on the acquired PET data. To extract respiratory signals, respiratory motion must be present in the PET data (*19*). Therefore, we verified the accuracy of quantification in a region where no respiratory motion was assumed using a $^{68}$Ge cylinder phantom, and we found that SUVmean and quantification accuracy were comparable to Static. SUVmax was slightly higher for

OncoFreeze AI than for Static, but the change in SUVmax with increasing bed speed was the same for Static and OncoFreeze AI (Table 1). These results indicate that OncoFreeze AI improved the effects of respiratory motion without compromising quantitative accuracy in the absence of respiratory motion. There are some limitations to our study. Though the image quality and other semiquantitative parameters improve, its clinical impact on patient management needs further evaluation. The present technique not only improves detection of lung lesions but may also improve detection of subdiaphragmatic hepatic lesions which is a potential additional advantage but not studied in the present study.

One of the features of PET/CT with CBM mechanism, such as Biograph Horizon, is the whole-body dynamic imaging function. At present, dynamic images from whole-body dynamic imaging cannot be combined with OncoFreeze AI; however, when this is realized, it will be useful (*23–27*). OncoFreeze AI eliminates the need to attach the device to the patient, which leads to shorter exam times for the patient and reduced radiation exposure for the operator. Respiratory gating reconstruction that takes into account the effects of respiratory motion is expected to make a significant contribution to SUV and harmonization, which are widely used in clinical studies of lung cancer (*28, 29*). This study demonstrates the usefulness of OncoFreeze AI, which enables device-less correction of respiratory motion effects on the Biograph Horizon, a popular PET/CT system.

## Conclusions

OncoFreeze AI, which does not require a device, can calculate SUV values and metabolic volumes comparable to OncoFreeze, which uses a device to measure respiratory motion.

OncoFreeze AI provides more accurate lung lesion images with significantly larger SUV values and smaller metabolic volumes compared to Static.

**Acknowledgements**

The authors wish to thank Nagara Tamaki, Shigenori Matsushima, Maki Kiba, (Department of Radiology, Graduate School of Medical Science, Kyoto Prefectural University of Medicine, Kyoto, Japan), and Koki Shirako, Azusa Tahata (Department of Radiological Technology, University Hospital, Kyoto Prefectural University of Medicine, Kyoto, Japan) for their contributions to this report.

**Funding** There is no funding for this study.

## Declarations

**Conflict of interest** All authors declare that they have no conflict of interest.

**Ethical approval** All procedures performed in studies involving human participants were in accordance with the ethical standards of the institutional and national research committee and with the 1964 Helsinki Declaration and its later amendments or comparable ethical standards. No animals were used in the present study by any author. Informed consent Based on the Ethical Guidelines for Medical and Health Research Involving Human Subjects of the Ministry of Health, Labour and Welfare, a waiver of informed consent for the retrospective analyses of the anonymized clinical data in this study was obtained from the Institutional Review Board of Kyoto Prefectural University of Medicine, Japan.

KEY POINT

QUESTION: Is a commercialized data-driven device-less respiratory gating application useful for evaluating lung lesion accumulation in continuous bed motion FDG-PET?

PERTINENT FINDINGS: Data-driven respiratory gating was performed in 38 lung lesions in a continuous bed motion FDG-PET study and showed a significant increase in SUV and decrease in MTV compared to not gating. Although data-driven, deviceless respiratory gating reconstruction assumes the presence of respiratory motion, the phantom test results did not impair the quantification of regions where respiratory motion was absent.

IMPLICATIONS FOR PATIENT CARE: Data-driven device-less respiratory gating reconstruction for evaluation of lung lesions in continuous bed motion FDG-PET can properly evaluate FDG accumulation.

## References


1. Brink1 I, Schumacher T, Mix1 M, et al. Impact of $^{18}$F-FDG-PET on the primary staging of small cell lung cancer. *Eur J Nucl Med Mol Imaging*. 2004;31:1614–20.
2. Verhagena AF T, Bootsma GP, Tjan-Heijnenc VCG, et al. FDG-PET in staging lung cancer How does it change the algorithm? *Lung Cancer*. 2004;44:175–81.
3. Garcı´a Vicente AM, Soriano Castrejo´n AM, Talavera Rubio MP, et al. $^{18}$F-FDG PET-CT respiratory gating in characterization of pulmonary lesions: approximation towards clinical indications. *Ann Nucl Med*. 2010;24:207–14.
4. Lupi A, Zaroccolo M, Salgarello M, Malfatti V, Zanco P. The effect of $^{18}$F-FDG-PET/CT respiratory gating on detected metabolic activity in lung lesions. *Ann Nucl Med*. 2009;23:191–96.
5. Callahan J, Binns D, Dunn L, Kron T. Motion effects on SUV and lesion volume in 3D and 4D PET scanning. *Australas Phys Eng Sci Med*. (2011) 34:489–95.
6. Robin P, Bourhis D, Bernard B, et al. Feasibility of systematic respiratory-gated acquisition in unselected patients referred for 18F-fluorodeoxyglucose positron emission tomography/computed tomography. *Front. Med*. 5:36. doi: 10.3389/fmed.2018.00036.
7. Seppenwoolde Y, Shirato H, Kitamura K, et al. Precise and real-time measurement of 3D tumor motion in lung due to breathing and heartbeat, measured during radiotherapy. *Int J Radiat Oncol*

*Biol Phys*. 2002;53(4): 822-34.

8. Knybel L, Cvek J, Molenda L, Stieberova N, Feltl D. Analysis of lung tumor motion in a large sample: patterns and factors influencing precise delineation of internal target volume. *Int J Radiat Oncol Biol Phys*. 2016;96(4):751–8.
9. Martin A. Repeatability of SUV in oncologic $^{18}$F-FDG PET. *J Nucl Med* 2017; 58:523–532.
10. Nehmeh SA, Erdi YE, Ling CC, Rosenzweig KE, Schoder H, Larson SM. Effect of respiratory gating on quantifying PET images of lung cancer. *J Nucl Med*. 2002;43:876–81.
11. Werner MK, Parker JA, Kolodny GM, English JR, Palmer MR. Respiratory gating enhances imaging of pulmonary nodules and measurement of tracer uptake in FDG PET/CT. *AJR.* 2009;193:1640–45.
12. Pösse S, Büther F, Mannweiler D, et al. Comparison of two elastic motion correction approaches for whole-body PET/CT: motion deblurring vs gate-to-gate motion correction. *EJNMMI Physics.* (2020) 7:19.
13. Walker MD, Morgan AJ, Bradley KM, McGowan DR. Data-Driven respiratory gating outperforms device-based gating for clinical $^{18}$F-FDG PET/CT. *J Nucl Med*. 2020;61:1678–83.
14. Schleyer P J, O'Doherty M J, Barrington S F, Marsden P K. Retrospective data-driven respiratory gating for PET/CT. *Phys Med Biol*. 2009;54(7):1935–50.
15. Kesner A L, Bundschuh R A, Detorie N C, et al. Respiratory gated PET derived in a fully automated manner from raw PET data. *IEEE Trans Nucl Sci*. 2009;56(3):677–86.

16. Buther F, Dawood M, Stegger L, et al. List mode–driven cardiac and respiratory gating in PET. *J Nucl Med.* 2009;50:674–81.

17. Walker MD, Morgan AJ, Bradley KM, McGowan DR. Evaluation of data-driven respiratory gating waveforms for clinical PET imaging. *EJNMMI Research*. (2019) 9:1.

18. Büther F, Jones J, Seifert R, Stegger L, Schleyer P, Schäfers M. Clinical evaluation of a data-driven respiratory gating algorithm for whole-body PET with continuous bed motion. *J Nucl Med*. 2020;61:1520–27.

19. Jones J, Hamill J, Fuerst S, Schleyer P, Hong I. White paper OncoFreeze AI deviceless motion management for PET imaging. *Siemens Healthcare GmbH*. 2020:1–21.

20. Kanda Y. Investigation of the freely available easy-to-use software 'EZR' for medical statistics. *Bone Marrow Transplant*. 2013;48:452–58.

21. Dias1 AH, Schleyer P, Vendelbo MH, Hjorthaug K, Gormsen LC, Munk OL. Clinical feasibility and impact of data-driven respiratory motion compensation studied in 200 whole-body 18F-FDG PET/CT scans. *EJNMMI Res earch*. (2022) 12:16.

22. Meier1 JG, Wu CC, Cuellar SLB, et al. Evaluation of a novel elastic respiratory motion correction algorithm on quantification and image quality in abdominothoracic PET/CT. *J Nucl Med*. 2019;60:279–284.

23. Nishimura M, Tamaki N, Matsushima S, et al. Dynamic whole-body 18F-FDG PET for

differentiating abnormal lesions from physiological uptake. *Eur J Nucl Med Mol Imaging*. 2020;47:2293–300.

24. Kotani T, Nishimura M, Tamaki N, et al. Comparison between dynamic whole-body FDG-PET and early-delayed imaging for the assessment of motion in focal uptake in colorectal area. *Ann Nucl Med*. (2021) 35:1305–11.

25. Nii T, Hosokawa S, Shirako K, et al. Achievements of true whole-body imaging using a faster acquisition of the lower extremities in variable-speed continuous bed motion. *Rad Phy Tech*. (2021) 14:373–80.

26. Naganawa M, Gallezot JD, Shah V, et al. Assessment of population-based input functions for Patlak imaging of whole body dynamic $^{18}$F-FDG PET. *EJNMMI Physics*. (2020) 7:67.

27. Osborne DR, Acuff S. Whole-body dynamic imaging with continuous bed motion PET/CT. *Nuclear Medicine Communications*. (2016) 37 (4):428–431.

28. Berghmans T, Dusart M, Paesmans M, et al. Primary tumor standardized uptake value (SUVmax) measured on fluorodeoxyglucose positron emission tomography (FDG-PET) is of prognostic value for survival in non-small cell lung cancer (NSCLC) a systematic review and meta-analysis (MA) by the European lung cancer working party for the IASLC lung cancer staging project. *J Thorac Oncol*. 2008;3:6 –12.

29. Houdu B, Lasnon C, Licaj I, et al. Why harmonization is needed when using FDG PET/CT as a

prognosticator: demonstration with EARL-compliant SUV as an independent prognostic factor in lung cancer. *Eur J Nucl Med Mol Imaging*. (2019) 46:421–28.

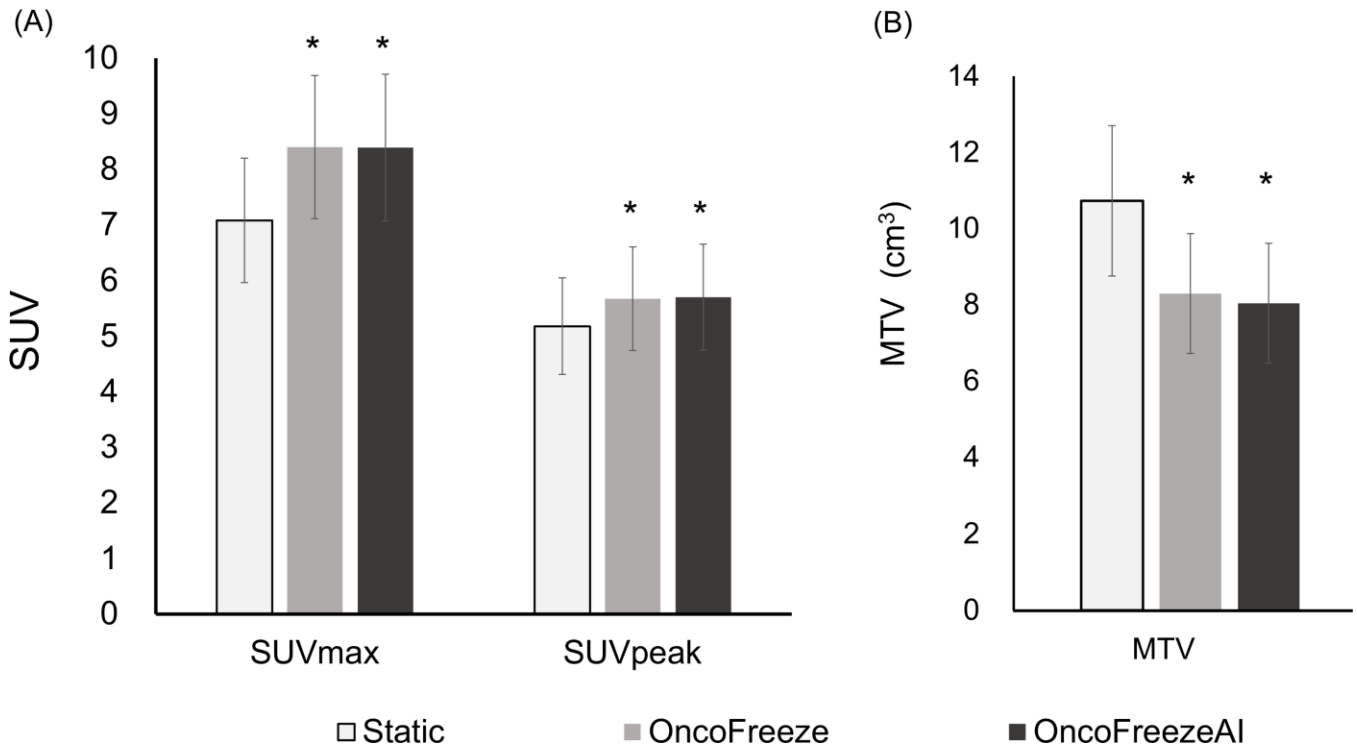


**Figure 1**: (A) SUVmax and SUVpeak and (B) MTV for Static, OncoFreeze and OncoFreeze AI.

* $P < 0.001$ for Static

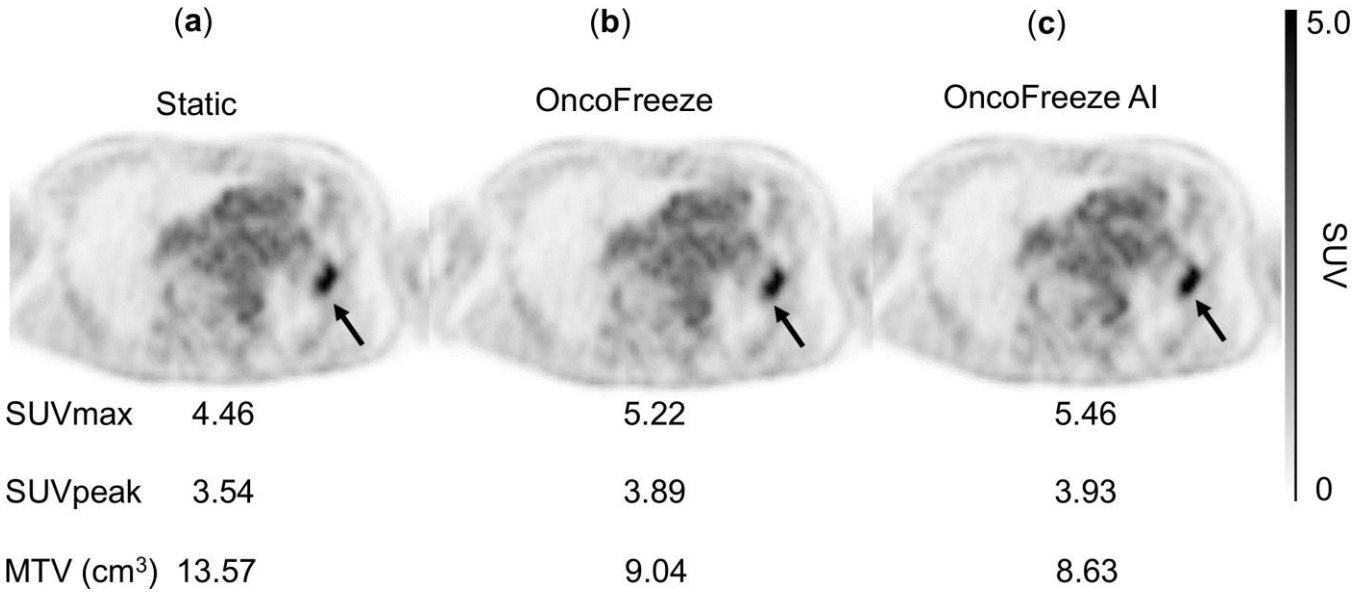


**Figure 2**: A 64-year-old male with left upper lobe lung cancer; 175.8cm, 76.0kg, $^{18}$F-FDG dose 2.99MBq/kg. PET images, transverse. SUVmax, SUVpeak, and MTV.

**a** Static, **b** OncoFreeze, **c** OncoFreeze AI

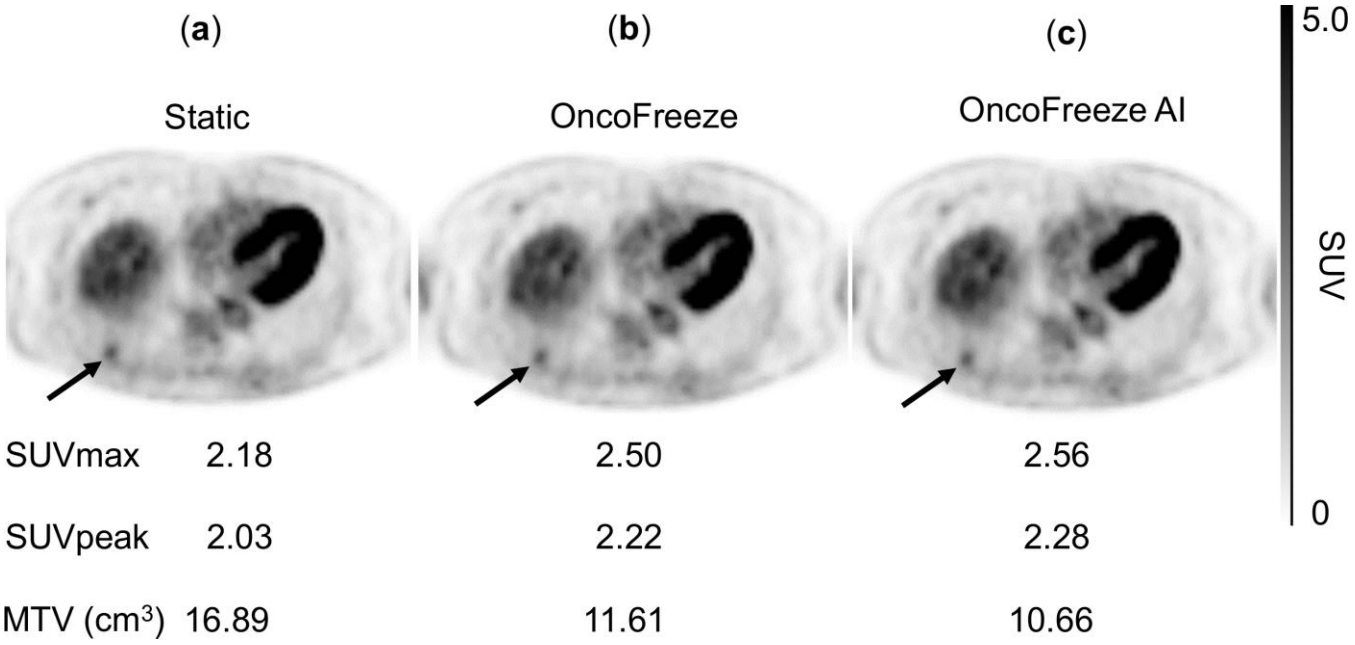


**Figure 3**: A 77-year-old female with right lower lobe lung cancer; 153.5cm, 56.7kg, $^{18}$F-FDG dose 3.26MBq/kg. PET images, transverse. SUVmax, SUVpeak, and MTV.

**a** Static, **b** OncoFreeze, **c** OncoFreeze AI

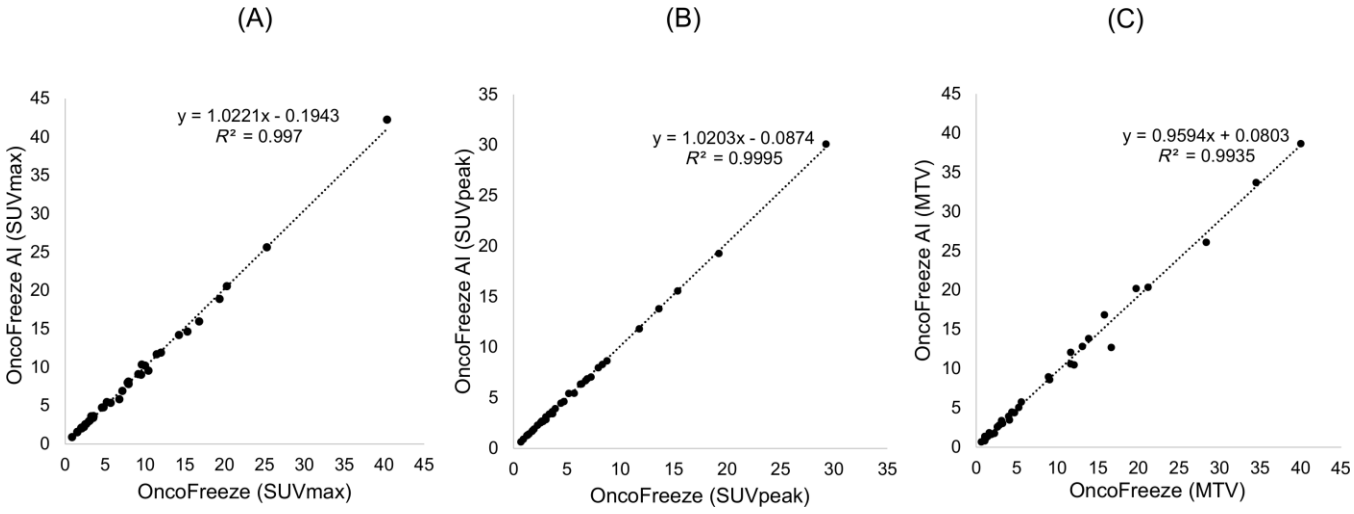


**Figure 4**: Correlation of OncoFreeze and OncoFreeze AI for SUVmax(A), SUVpeak(B) and MTV(C)

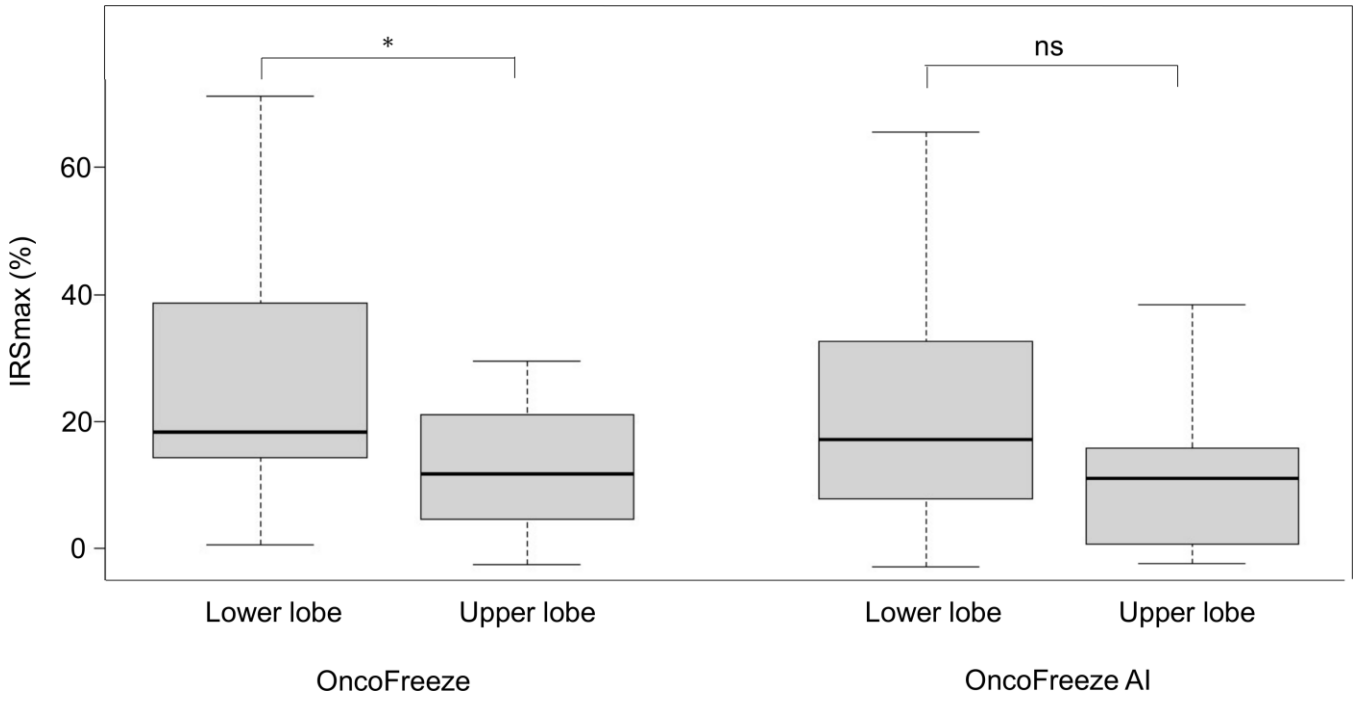


**Figure 5**: The ratios of SUVmax (IRSmax) from Static to OncoFreeze and OncoFreeze AI for 18 upper lobe and 15 lower lobe lesions. * $P = 0.0273$

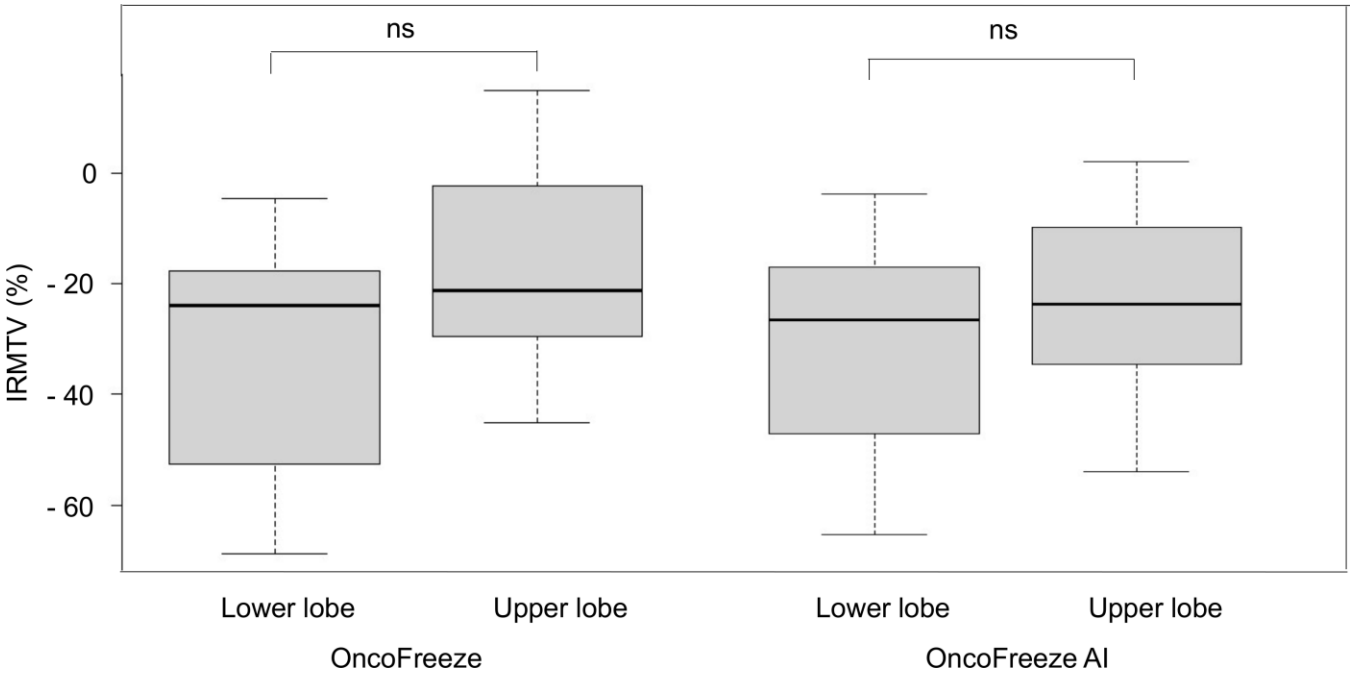


**Figure 6**: The ratios of MTV (IRMTV) from Static to OncoFreeze and OncoFreeze AI for 18 upper lobe and 15 lower lobe lesions.

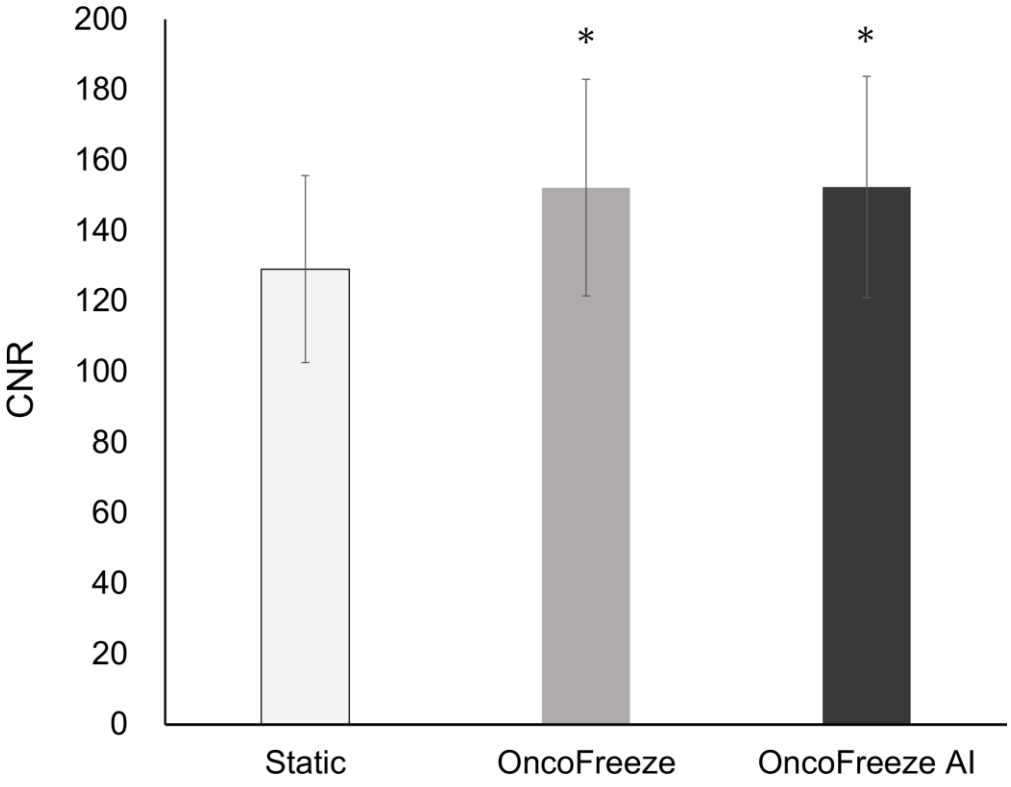


**Figure 7**: Static and OncoFreeze and OncoFreeze AI in contrast-to-noise ratio (CNR).

* $P < 0.001$ for Static

Table 1 Relationship between bed motion speed, radioactivity concentration, and SUV in a $^{68}$Ge cylinder phantom

| | Activity (kBq/mL) | | SUV (mean) | | SUV (sd) | | SUV (max) | |
|---|---|---|---|---|---|---|---|---|
| Bed speed (mm/s) | Static | OncoFreeze AI | Static | OncoFreeze AI | Static | OncoFreeze AI | Static | OncoFreeze AI |
| 0.6 | 9.05 | 9.03 | 1.04 | 1.04 | 0.04 | 0.04 | 1.22 | 1.28 |
| 0.9 | 9.06 | 9.02 | 1.04 | 1.04 | 0.05 | 0.06 | 1.25 | 1.33 |
| 1.2 | 9.05 | 9.02 | 1.04 | 1.04 | 0.05 | 0.06 | 1.31 | 1.39 |
| 1.5 | 9.07 | 9.04 | 1.04 | 1.04 | 0.06 | 0.07 | 1.34 | 1.38 |
| 1.8 | 9.06 | 9.02 | 1.04 | 1.04 | 0.07 | 0.08 | 1.44 | 1.50 |
| 2.1 | 9.08 | 9.04 | 1.05 | 1.04 | 0.07 | 0.09 | 1.44 | 1.50 |
| 2.4 | 9.06 | 9.00 | 1.04 | 1.04 | 0.08 | 0.10 | 1.42 | 1.55 |
| 2.7 | 9.07 | 9.01 | 1.04 | 1.04 | 0.08 | 0.10 | 1.47 | 1.52 |
| 3.0 | 9.07 | 8.99 | 1.04 | 1.04 | 0.09 | 0.10 | 1.43 | 1.59 |

Graphical Abstract